stellarator news

Published by Fusion Energy Division, Oak Ridge National Laboratory
Building 9201-2 P.O. Box 2009 Oak Ridge, TN 37831-8071, USA

Editor: James A. Rome Issue 72 November 2000
E-Mail: jar@ornl.gov Phone (865) 574-1306
On the Web at *http://www.ornl.gov/fed/stelnews*

Physics issues for compact drift-optimized stellarators

Introduction

Stellarator optimization techniques have allowed the exploration of design parameters corresponding to compact (aspect ratio $R_0/\langle a\rangle$ = 2.5–4), low-field-period (N_{fp} = 2–4) toroidal devices with attractive physics properties. (Here angle brackets around variables represent volume averages.) These configurations permit near-term experiments with the same plasma minor radius $\langle a\rangle$ as the more conventional large-aspect-ratio stellarators at lower cost. In addition, they offer the longer-term potential of a more economically sized, higher-power density fusion reactor. These devices will also explore new regimes of stellarator parameter space in which the transport physics, equilibrium resilience, plasma flow dynamics, radio-frequency (RF) heating strategies, and microturbulence are expected to be quite different than at higher aspect ratios.

The strong geometric couplings that occur at lower aspect ratios generally require a numerical approach and present challenging computational problems because of the broad spectra of $|\mathbf{B}|$ (in Fourier space) that must be considered. We have used a transport optimization strategy based on quasiomnigeneity (QO) [1, 2] that minimizes particle drifts by targeting both the variation of the longitudinal adiabatic invariant J within magnetic flux surfaces and local neoclassical transport rates as calculated by the DKES [3] code. Additional optimization targets are Mercier stability, ballooning stability based on the COBRA [4, 5] code, a self-consistent bootstrap current that is reduced (by factors > 3) from that in a tokamak, and rotational transform profiles that avoid major resonances.

Previously [2], we analyzed 3- and 4-field-period QO configurations which were close to quasihelically symmetrical states for $R_0/\langle a\rangle$ = 3.5–4. Here we focus on 2- and 3-field-period devices that are close to quasipoloidally symmetrical states for $R_0/\langle a\rangle$ = 2.5–3.5. The emergence of this form of quasisymmetry has been a natural outcome of directing our QO optimization approach toward lower N_{fp} and lower $R_0/\langle a\rangle$. Quasipoloidal symmetry offers the unique property of minimizing the viscous damping (caused by magnetic pumping) in the direction of the $\mathbf{E}_r \times \mathbf{B}$ drift. This feature may be important in accessing enhanced confinement regimes that depend on $\mathbf{E}_r \times \mathbf{B}$ shear and should lead to much lower parallel flows than in quasiaxisymmetric devices [6].

Two types of configurations have emerged from our optimization studies. The first, which we regard as more appropriate for a near-term experiment, relies on plasma shaping to achieve most of its rotational transform and quasipoloidal symmetry. The second, which we regard as a longer-term option because of its more challenging startup and heating requirements, derives most of its transform and quasisymmetry from bootstrap currents driven by the finite volume-averaged plasma pressure $\langle\beta\rangle$. In this respect it resembles an advanced tokamak, but because of its quasipoloidal symmetry the bootstrap current is spatially well aligned and is lower (by a factor of 3 or 4) than that of the equivalent tokamak. This latter feature leads to higher $\langle\beta\rangle$

In this issue . . .

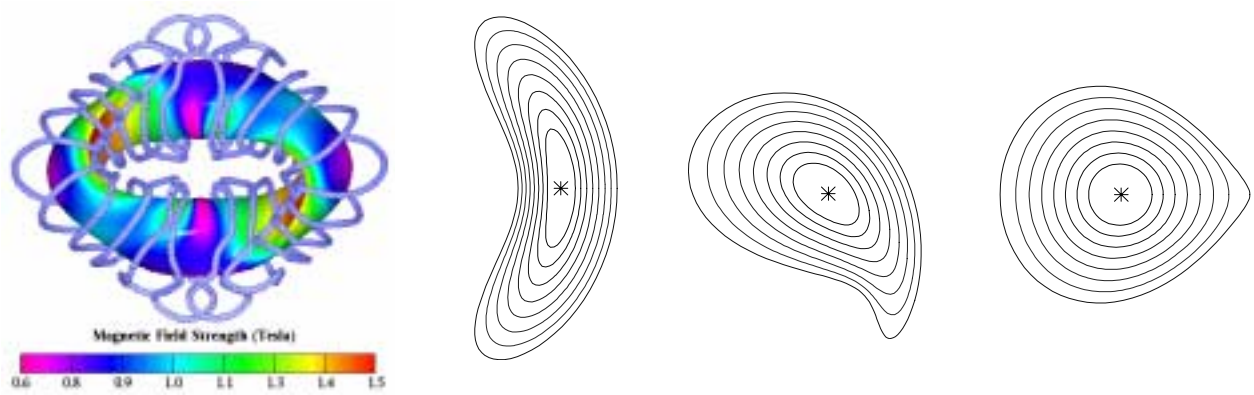

Fig. 1. (a) Top view of outer flux surface and modular coils (in blue) for an $N_{fp} = 2$, $R_0/\langle a \rangle = 2.5$ device. (b)–(d) VMEC flux surfaces at toroidal angles $\zeta/N_{fp} = 0°$, 90°, and 180°.

stability toward external kink and vertical modes than in the advanced tokamak.

Low-⟨β⟩, near-.term experimental configuration

In Fig. 1 we show the flux surface shapes and coils for a 2-field-period, $R_0/\langle a \rangle = 2.5$ device, which is of the first type mentioned above.

The rotational transform profiles with and without bootstrap current and the Fourier coefficients B_{mn} of $|\mathbf{B}|$ are shown in Fig. 2. As previously indicated, these devices are dominantly quasipoloidal [i.e., the $m = 0$ components (0,0), (0,1), and (0,2) of B_{mn} are the largest] and most of their rotational transform is provided by the external coils. The bootstrap current flows in the direction that increases the transform; this fact, coupled with the positive shear in the transform, provides stabilization against neoclassical tearing instabilities. The threshold for ballooning instabilities is $\langle \beta \rangle = 1.8$–2%.

We have used pressure profiles with zero gradient at the plasma edge to avoid creating finite bootstrap currents at the edge; such edge currents are not thought to be maintainable but can lead, in some cases, to higher ballooning thresholds (although the kink mode should be destabilized). Predicted levels of bootstrap current (in the low-collisionality limit) for this device are about a third of those in the equivalent tokamak configuration. For example, in a $\langle B \rangle = 1$ T, $R_0 = 0.8$ m device at $\langle \beta \rangle = 1.5\%$, 34 kA of bootstrap current would flow, based on the low collisionality limit. Calculations of bootstrap current for collisionalities representative of experimental conditions (see Table 1) are under way using the DKES model [3]; preliminary results indicate that the bootstrap current will be reduced (~1/3) from the low collisionality limit and will depend weakly on the value of the ambipolar electric field.

Our analysis of neoclassical transport in this device has been directed at regimes that would be accessible in a

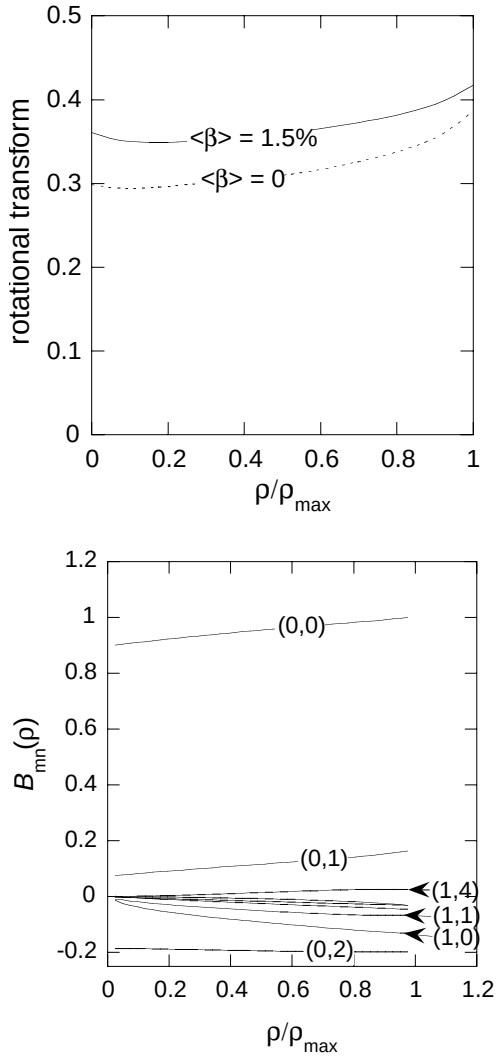

Fig. 2. Rotational transform profiles (top) and B_{mn} amplitudes (bottom) vs toroidal flux. The poloidal and toroidal mode numbers (m, n) are indicated for the larger components of B_{mn}.

Table 1. Plasma parameters for a device with $\langle B \rangle$ = 0.5–1 T, R_0 = 0.83 m, and N_{fp} = 2, based on ISS95 scaling with enhancement factor h = 1.

Case	Heating/ Magnetic field	Density (10^{20} m^{-3})	T_e, T_i (keV)	ν^*_e, ν^*_i	$\langle \beta \rangle$ (%)
(a)	0.5-MW ECH, B = 1 T	0.18	1.4, 0.15	0.02, 1.6	0.7
(b)	1-MW ECH, B = 0.5 T	0.045	2.1, 0.2	0.002, 0.22	1
(c)	1-MW ICH, B = 1.0 T	0.83	0.5, 0.5	0.68, 0.64	2
(d)	1-MW ICH, B = 0.5 T	0.59	0.4, 0.25	0.75, 1.8	3.7

$\langle B \rangle$ = 1 T, R_0 = 0.8 m device with 28-GHz (B = 0.5 T) and 53-GHz (B = 1 T) electron cyclotron heating (ECH) sources available. The impact of 1 MW of supplementary ion cyclotron heating (ICH), which is available in the 40- to 80-MHz range, has also been considered; this would allow access to higher density regimes than ECH (density cutoff limited).

Our transport analysis has been carried out with the DELTA5D Monte Carlo model, which is a generalization of an earlier stellarator Monte Carlo code [7] to include energetic beam and alpha populations, ICH, global lifetime estimates, and bootstrap current options. Populations of ions and electrons are initially distributed randomly in pitch angle and in poloidal and toroidal angles. The radial distribution is consistent with a flat density profile, while the energy distribution is modeled after parabolic-squared temperature profiles. As particles leave the outer flux surface boundary, they are replaced with new initial values chosen from these distributions.

We assume an ion-root ambipolar potential profile that rises from the center inversely with the drop-off in electron temperature profile and take $e\phi/kT_e = 1$ at the plasma edge. Electron-root profiles ($e\phi/kT_e < 0$) have also been examined for the ECH cases; however, for the same edge value of $|e\phi/kT_e|$, these cases lead to nearly the same global confinement times as the ion root.

We are also developing a self-consistent calculation of the electric field using the DKES model [3], similar modeling [8] carried out for the W7-AS experiment. Initial results from these calculations near the plasma edge show ion-root behavior with $e\phi/kT_e \sim 1$. Table 1 lists the parameters we have considered for the various heating scenarios (here we assume $Z_{eff} = 1$).

Applying the Monte Carlo transport model these parameters leads to the predicted neoclassical lifetimes presented in columns 2–4 of Table 2. Column 5 compares the predictions with the ISS95 [9] empirical stellarator confinement scaling, assuming no enhancement factor (here $\tau_{E,global}$ is the overall neoclassical energy lifetime, taking into account both $\tau_{E,ion}$ and $\tau_{E,elec}$). The neoclassical loss rates are considerably smaller than the ISS95 rates, especially at the higher range of densities that can be accessed with ICH.

Table 2. Predicted neoclassical lifetimes (columns 2, 3, 4) for the cases of table 1 and their relation to ISS95 stellarator scaling with enhancement factor h = 1.

	Predicted lifetime (ms)				
Case	$\tau_{E\ ion}$	$\tau_{E,elec}$	$\tau_{E,global}$	$\tau_{E,ISS95}$	$\tau_{E,global}/\tau_{E,ISS95}$
(a)	16.2	17.4	16.2	8.1	2
(b)	4.3	1.95	2.1	1.5	1.4
(c)	27	~100	41.7	11.7	3.6
(d)	7.7	~55	16.4	5.5	3

Free boundary and field line following calculations have also been carried out for the modular coil set shown in Fig. 1 in order to check that a good reconstruction of flux surfaces is obtained and that neoclassical confinement is preserved. Monte Carlo energy lifetimes based on free boundary equilibria show less than a 10% change from the original fixed boundary results. Also, analysis of this configuration with the PIES [10] code up to $\langle \beta \rangle$ = 1.6% indicates that only a minimal loss of flux surfaces occurs over the outer 10% of the plasma radius.

High $\langle \beta \rangle$ Configurations

In addition to the device described above, we have also found nearly quasipoloidal configurations with N_{fp} = 2 and 3 ($R_0/\langle a \rangle$ = 2.7–3.7) in which the plasma bootstrap current supplies a large fraction of the transform. In the case of 3 field periods, these devices fully access the second regime for ballooning stability at around $\langle \beta \rangle$ > 15% with stabilization entering from the outer region of the plasma at $\langle \beta \rangle$ = 6–7%. Configurations with N_{fp} = 2 that achieve second regime stabilization for $\langle \beta \rangle$ as low as 1% have also been found. Vertical and external kink modes are weakly unstable at $\langle \beta \rangle$ = 15% and can be stabilized by a very small reduction (10%) of the self-consistent bootstrap current. However, these modes are sufficiently near marginal stability that a slight modification in the three-dimensional (3-D) shape should also provide stabilization. An example of a 3-field-period configuration of this type is shown in Fig. 3 along with its transform profile ι with and without plasma bootstrap currents.

At this relatively low value of ι, the collisionless bootstrap current in this device is about a quarter of that in the equiv-

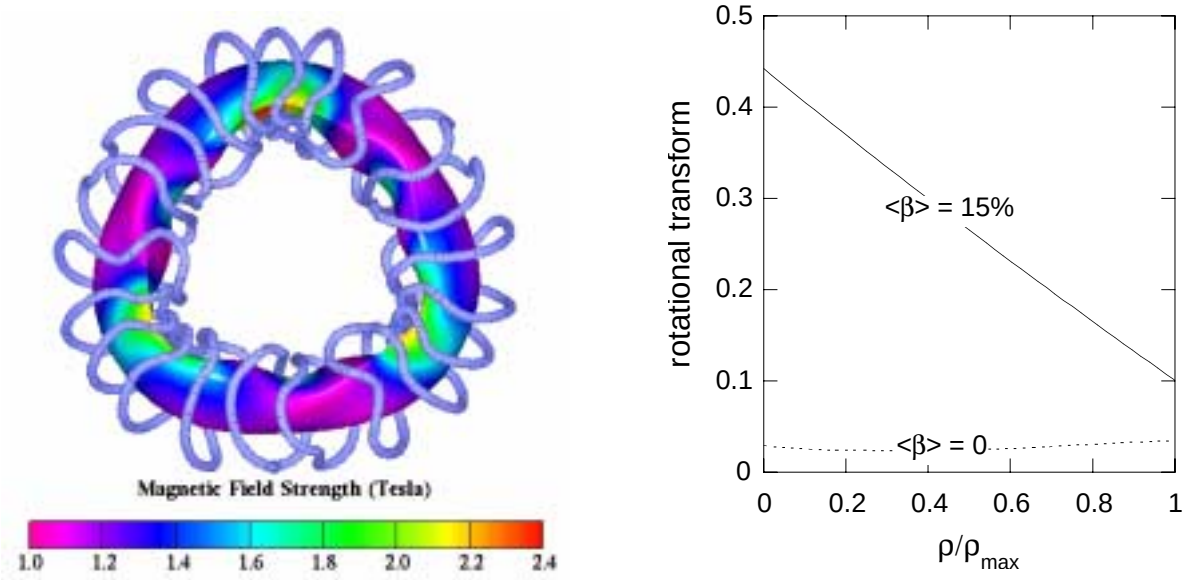

Fig. 3. Top view of outer flux surface with modular coils (in blue) for an $N_{fp} = 3$, $R_0/\langle a \rangle = 3.7$ device (left) and its rotational transform profiles (right), with (top) and without bootstrap current.

alent tokamak. These configurations have tokamak-like transform profiles and approach quasipoloidal symmetry with increasing ⟨β⟩. This feature is evident in the B_{mn} spectrum shown in Fig. 4(a), where the $n = 0$ [(0,0), (0,1), and (0,2)] components of B_{mn} may be seen to dominate.

At such high values of ⟨β⟩, the |**B**| contours also become poloidally closed (at fixed toroidal cross sections) and begin to align with flux surfaces. This is a further indication of the enhancement in quasipoloidal symmetry associated with increasing ⟨β⟩. As may be seen from Fig. 4(a), the $B_{0,0}$ component is depressed in the center; this is a result of the diamagnetic well (shift due to Pfirsch-Schlüter currents) at this value of ⟨β⟩. The poloidal gradient *B* drifts associated with this radial variation in $B_{0,0}$ are helpful for containing energetic particles, as shown for alpha particles in Fig. 4(b). Here the curve labeled "base configuration" is constrained to have the same outer flux surface shape and transform profile as the ⟨β⟩ = 23% case, but it does not include the plasma diamagnetic current effects that lead to the modified B_{mn} spectrum shown in Fig. 4(a) (i.e., this is essentially a ⟨β⟩ = 0 case, except that an ad hoc plasma current is provided, equal to the bootstrap current of the ⟨β⟩ = 23% case). The alpha energy losses (~ 12%) at the highest ⟨β⟩ are the lowest we have found in modeling any of this class of compact stellarator devices.

Conclusions

We have found attractive compact stellarators with $N_{fp} = 2$ and 3 and aspect ratios $R_0/\langle a \rangle = 2.5 – 3.5$ that maintain good neoclassical confinement by approaching quasipoloidal symmetry. These configurations can be produced by relatively simple modular coils, from which we have verified flux surface reconstruction and which retain the confinement properties of the original fixed boundary equilibrium. Two types of compact stellarator configurations have been examined: one that produces most of the rotational transform and quasipoloidal symmetry through external means and a second that relies more heavily on the plasma currents associated with high plasma ⟨β⟩ to produce these effects. We envision the first type of configuration to be a candidate for a near-term experiment with $B \sim 1$ T and $R_0 \sim 1$ m. Our transport analysis has shown that such a device has an adequate margin of confinement above ISS95 scaling (up to 3.6 times ISS95). The second type of device, which may form the basis for a reactor vision of a compact QO stellarator, is computed to achieve very high ⟨β⟩ limits (~15%) for a low-aspect-ratio stellarator and very good (tokamak-like) energetic alpha particle confinement.

Acknowledgement

This research was sponsored by the Office of Fusion Energy, U.S. Department of Energy, under contract DE-AC05-00OR22725 with UT-Battelle, LLC, and contract DE-AC020-76-CHO3037 with Princeton Plasma Physics Laboratory.

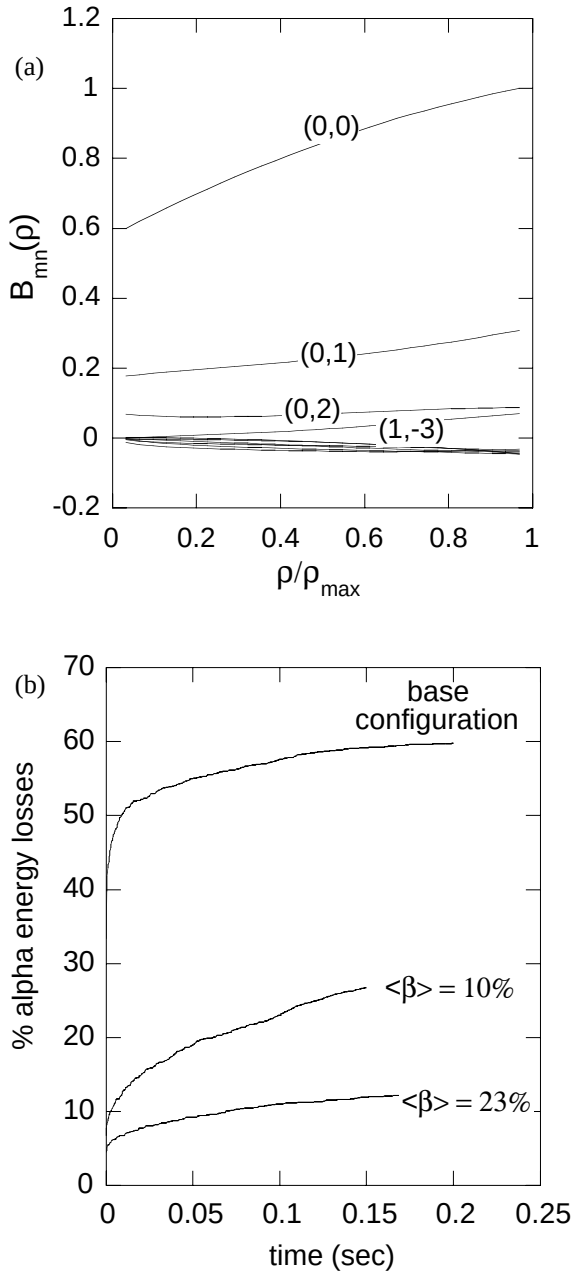

Fig. 4. (a) B_{mn} amplitudes vs toroidal flux for a $\langle\beta\rangle$ = 23%, N_{fp} = 3 device. (b) Fraction of 3.5-MeV alpha particle losses for a reactor-scale version (R_0 =10 m, $\langle B\rangle$ = 5 T) of this device with increasing $\langle\beta\rangle$.

D. A. Spong, S. P. Hirshman, L. A. Berry, J. F. Lyon, R. H. Fowler, D. J. Strickler, M. J. Cole, B. E. Nelson, D. E. Williamson
Oak Ridge National Laboratory
P. O. Box 2009, Oak Ridge, TN 37831-8071
E-mail: spongda@ornl.gov

A. S. Ware, D. Alban
University of Montana, Missoula, MT

R. Sanchez
Universidad Carlos III de Madrid, Madrid, Spain

G. Y. Fu, D. A. Monticello
Princeton Plasma Physics Laboratory, Princeton, NJ

W. H. Miner, Jr., P. M. Valanju
University of Texas, Austin, TX

References

[1] S.P. Hirshman, D. A. Spong, J. C. Whitson, et al., Phys. Plasmas **6** (1999) 1858.

[2] D. A. Spong, S. P. Hirshman, J. C. Whitson, et al., Nuc. Fusion **40** (2000) 563.

[3] W. I. Van Rij, and S. P. Hirshman, Phys. Fluids **B1** (1989) 563.

[4] R. Sanchez, S. P. Hirshman, J. C. Whitson, and A. S. Ware, J. Comput. Phys. **161** (2000) 576.

[5] R. Sanchez, S. P. Hirshman, A. S. Ware, L. A. Berry, and D. A. Spong, Plasma Phys. Controlled Fusion **42** (2000) 641.

[6] G. H. Neilson, A. H. Reiman, et al., Phys. Plasmas **7** (2000) 1911.

[7] R. H. Fowler, J. A. Rome, and J. F. Lyon, Phys. Fluids **28** (1985) 338.

[8] J. Baldzuhn, M. Kick, H. Maassberg, and W7-AS Team, Plasma Phys. Controlled Fusion **40** (1998) 967.

[9] U. Stroth et al., Nucl. Fusion **36** (1996) 1063.

[10] A. Reiman, H. Greenside, J. Comput. Phys. **75** (1988) 1423.